Probing magnetic order in LiMPO$_4$ (M = Ni, Co, Fe) and lithium diffusion in Li$_x$FePO$_4$

P. J. Baker,[1,*] I. Franke,[2] F. L. Pratt,[1] T. Lancaster,[2] D. Prabhakaran,[2] W. Hayes,[2] and S. J. Blundell[2]
[1]*ISIS Facility, STFC Rutherford Appleton Laboratory, Chilton, Oxon OX11 0QX, United Kingdom*
[2]*Clarendon Laboratory, University of Oxford, Parks Road, Oxford OX1 3PU, United Kingdom*
(Received 10 August 2011; published 3 November 2011)

Muon spin relaxation measurements are reported on three members of the Li$_x$$MPO_4$ series. The magnetic properties of stoichiometric samples with M = Ni, Co, Fe were investigated at low temperature. In LiNiPO$_4$ we observe different forms of the muon decay asymmetry in the commensurate and incommensurate antiferromagnetic phases, accompanied by a change in the temperature dependence of the muon oscillation frequency. In LiCoPO$_4$ the form of the muon decay asymmetry indicates that the correlation between layers decreases as the Néel temperature is approached from below. LiFePO$_4$ shows more conventional behavior, typical for a three-dimensional antiferromagnet. Measurements on Li$_x$FePO$_4$ with $x = 0.8$,0.9, and 1 show evidence for lithium diffusion below ∼250 K and muon diffusion dominating the form of the relaxation at higher temperature. The thermally activated form of the observed hopping rate suggests an activation barrier for lithium diffusion of ∼100 meV and a diffusion constant of $D_{\mathrm{Li}} \sim 10^{-10}$ to 10^{-9} cm^2 s^{-1} at room temperature.

DOI: 10.1103/PhysRevB.84.174403 PACS number(s): 76.75.+i, 75.50.Ee, 82.47.Aa, 82.56.Lz

I. INTRODUCTION

The series of phosphates LiMPO$_4$ crystallize in the orthorhombic olivine structure, with layers of magnetic transition metal M ions that are relatively well coupled, meaning they are intermediate between two- and three-dimensional magnetism.[1,2] The choice of M ion allows the single-ion interactions to be tuned discretely and a range of magnetic behavior results. LiNiPO$_4$ shows commensurate antiferromagnetic order at low temperature and then undergoes a transition to incommensurate order just below the bulk ordering temperature.[2] Both LiCoPO$_4$ and LiNiPO$_4$ exhibit magnetoelectric behavior[3] and the resulting toroidal domains in LiCoPO$_4$ have been observed using optical measurements.[4]

A separate interest in this series of phosphates comes from their application as battery cathode materials. This is particularly relevant for LiFePO$_4$ which has a slightly lower cell voltage and energy density than the widely used LiCoO$_2$, but a significantly better lifetime, resistance to thermal runaway, and a smaller environmental impact.[5–9] The use of Li$_x$FePO$_4$ as a battery cathode material leads to questions concerning its electrochemical properties and the kinetics of lithium diffusion, both of which have received considerable study.[9] Both calculations and experiment have addressed the activation barriers for lithium ion and electron conduction, as well as the lithium ion diffusion rate.[10–24] While the calculated values have converged there are considerable variations in the results of experiments carried out using different techniques.

In this paper we present a muon-spin relaxation (μSR) investigation of the low-temperature magnetic properties of LiMPO$_4$ (M = Ni, Co, Fe) and the high-temperature diffusive properties of Li$_x$FePO$_4$ ($x = 0.8$, 0.9, 1.0). As well as being a sensitive probe of magnetic ordering,[25,26] μSR provides a means of investigating diffusion processes of both the muon[27] and other species that perturb its environment.[28] Lithium diffusion is a process that provides such a perturbation and μSR has now been applied to studying it in a wide range of battery cathode materials: Li$_x$[Mn$_{1.96}$Li$_{0.04}$]O$_4$,[29,30] Li$_{0.6}$TiO$_2$,[31] Li$_{3-x-y}$Ni$_x$N,[32] Li$_x$CoO$_2$,[28,33] and LiNiO$_2$.[34] Of these, the studies on Li$_x$CoO$_2$ have been the most extensive and found that the lithium diffusion rate in this compound is well suited to the time scale probed by μSR. Similar studies on a different time scale can be carried out using NMR.[24,35,36]

We describe the preparation of the samples and the general μSR technique in Sec. II, including the details of how the low-temperature data were analyzed. In Secs. III A, III B, and III C we present our μSR data and analysis. In Sec. IV we discuss the existing literature on lithium diffusion in Li$_x$FePO$_4$ and describe our higher temperature μSR experiments, data analysis, and results. Our conclusions are summarized in Sec. V.

II. EXPERIMENTAL METHOD

Powders of stoichiometric and Li-deficient Li$_x$$MPO_4$ (M = Ni, Co, and Fe; $x = 0.8$ and 0.9) were synthesized by the solid-state reaction technique. Starting materials of high purity (>99.99%) Li$_3$PO$_4$, NiO, Co$_3$O$_4$, Fe$_2$O$_3$, and NH$_4$H$_2$PO$_4$ were mixed and sintered in three stages: 175 °C for 10 h, 225 °C for 5 h, and 725 °C for 24 h. After grinding, they were sintered again at 750 °C for 24 h. Finally the powders were made into rods and sintered at 775 °C for 12 h. Single crystals of stoichiometric LiMPO$_4$ were grown in a four-mirror optical floating-zone furnace (Crystal System Inc.). The growth was carried out at a speed of 2–3 mm/h with the feed and seed rods counterrotating at 25 rpm. Crystals were grown in an argon pressure of 1–4 atm.

Spin-polarized positive muons were implanted into the samples where they stop at interstitial sites with large electronegativity and decay with a mean lifetime of 2.2 μs. While the muons remain within the sample their spin direction is affected by the local magnetic field at their stopping site, with the muon's gyromagnetic ratio $\gamma_\mu = 2\pi \times 135.5$ MHz T^{-1} being intermediate between those of the electron and proton. The muon spin polarization is followed as a function of time by measuring the asymmetry in the count rate of decay positrons, $A(t)$, in two detectors on opposite sides of the sample.[25] Our μSR experiments were carried out at the Paul Scherrer Institute using the General Purpose Surface-muon instrument (GPS) for the low-temperature measurements of the stoichiometric

 ©2011 American Physical Society

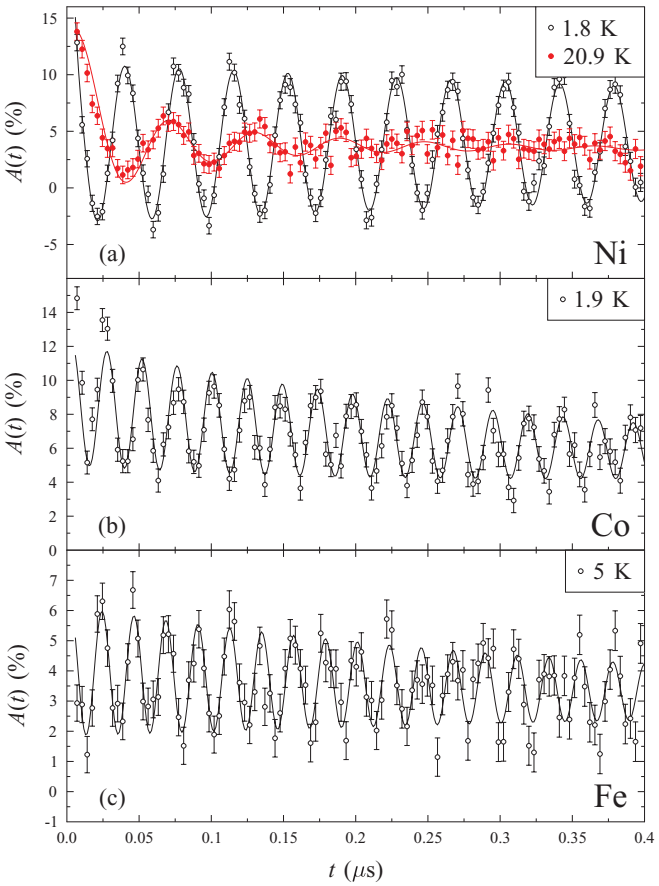

FIG. 1. (Color online) Muon decay asymmetry data for LiMPO$_4$: (a) M = Ni, (b) M = Co, and (c) M = Fe. Fits to the data are described in the text. The initial asymmetries are reduced from the values due to energy selection of decay positrons by including data from spatially segmented detectors giving better counting statistics.

crystalline samples and at the ISIS Facility using the MuSR spectrometer for the high-temperature measurements of the Li$_x$FePO$_4$ samples. For the low-temperature measurements, unaligned single crystals (∼5 × 5 × 1 mm) were placed in a 25 μm Ag foil packet and attached to a two-pronged sample holder so that muons not hitting the sample would be vetoed. For the high-temperature measurements, powder samples were placed inside 25 μm Ag foil packets (∼10 × 10 × 1 mm) on a silver backing plate.

The data shown in Fig. 1 and Fig. 5 were analyzed using the WiMDA program.[37] It was found that similar fitting functions were suitable for describing the low-temperature data on each of the three stoichiometric samples, based on the general form

$$A(t) = A_\perp e^{-\lambda t}\cos(2\pi f t + \phi) + A_\parallel e^{-\Lambda t} + A_{\rm bg}. \qquad (1)$$

The $A_\perp$ term describes an exponentially damped oscillation due to a quasistatic magnetic field perpendicular to the muon spin direction. Having corrected for apparent phases due to a partial muon spin rotation relative to the detectors, the phase ϕ could be fixed to zero in both the low-temperature commensurate phase of LiNiPO$_4$, and below $T_{\rm N}$ in LiFePO$_4$. In LiCoPO$_4$, ϕ was found to depend on temperature. The $A_\parallel$ term describes the exponential relaxation for muon spins with their direction along that of the local field at their stopping site, which are depolarized by spin fluctuations. The final term describes the temperature-independent contribution to the asymmetry from muons stopping outside the sample. Just above the magnetic ordering transition there is no oscillatory signal and, as is generally the case in paramagnets, the data are well described by an exponential relaxation, with rate Λ. This form of the data is not compatible with short-ranged static magnetic order persisting above the long-range magnetic ordering transition on the time scales probed by muons. We discuss the form of the muon depolarization at higher temperatures in Sec. IV.

In the incommensurate antiferromagnetic phase of LiNiPO$_4$ we found that Eq. (1) did not provide a satisfactory description of the data, even allowing ϕ to change from the value of zero found to describe the commensurate phase. For incommensurate magnetic phases, where the muons sample a significant range of magnetic fields, the oscillatory part of the muon relaxation function takes the form of a Bessel function,[26] so that $A(t)$ can be written as

$$A(t) = A_\perp e^{-\lambda' t} J_0(2\pi f' t) + A_\parallel e^{-\Lambda t} + A_{\rm bg}. \qquad (2)$$

For well-defined oscillation frequencies that varied continuously below $T_{\rm N}$ we fitted the temperature dependence to the phenomenological function

$$f(T) = f(0)[1 - (T/T_{\rm N})^\alpha]^\beta, \qquad (3)$$

where α describes the $T \to 0$ trend and β describes the trend approaching $T_{\rm N}$, giving a means of estimating the critical exponent of the magnetization, since the oscillation frequency f is linearly proportional to the sublattice magnetization.

III. LOW-TEMPERATURE RESULTS

A. LiNiPO$_4$

On cooling LiNiPO$_4$ orders incommensurately at $T_{\rm N}$ = 21.8 K, then orders commensurately at $T_{\rm IC-C}$ = 20.7 K.[2,38] Neutron diffraction has characterized both the long-range ordered phases and found diffuse scattering well above $T_{\rm N}$. The trend in the magnetic order parameter approaching the breakup of collinear order was found to follow the dependence expected for a 2D Ising model;[39] an anomalous correlation between the spin wave spectrum and the incommensurate magnetic order[40] and coexisting short- and long-range incommensurate magnetic order were reported for the intermediate phase.[2]

In LiNiPO$_4$ we can divide the data into three distinct temperature regions. At the lowest temperatures, below 20.7 K, we observe underdamped oscillations at a single frequency, with the data shown in Fig. 1(a) well described by Eq. (1) with $\phi = 0$. This is consistent with the commensurate magnetic structure determined by neutron diffraction.[2] The temperature dependence of the oscillation frequency f is shown in Fig. 2(a), the linewidth λ in 2(b), and the relaxation rate Λ in 2(c). The linewidth is relatively small compared to the oscillation frequency, as is evident from the persistence of the oscillations in the low-temperature data, and only grows slightly approaching the commensurate-incommensurate phase transition.

Between 20.7 and 21.8 K the oscillations persist, but their form changes from the cosinusoidal form described by Eq. (1)

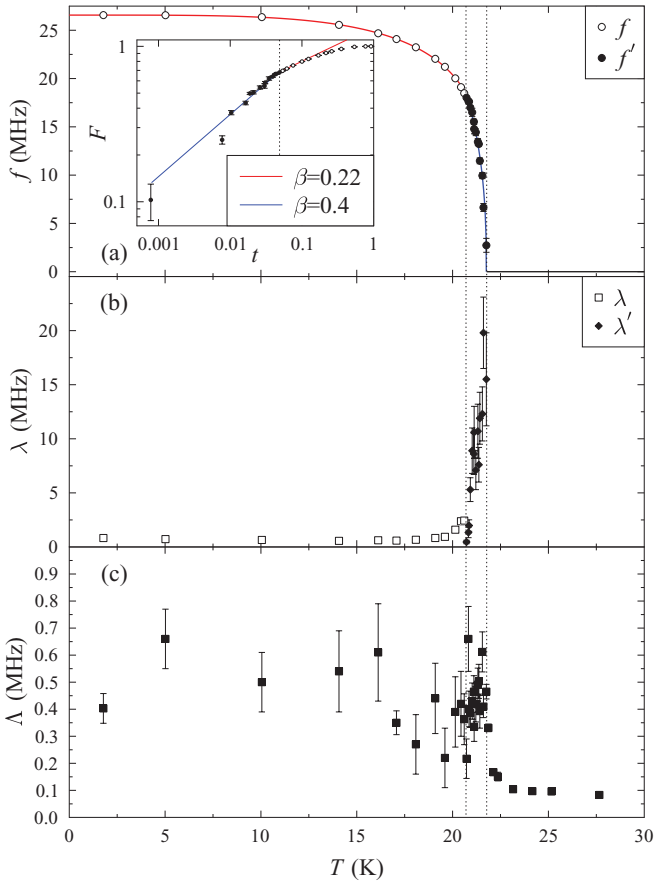

FIG. 2. (Color online) Parameters derived from fitting Eqs. (1) and (2) to the μSR data for LiNiPO$_4$ shown in Fig. 1(a). (a) Oscillation frequencies f and f'. Inset: Reduced oscillation frequency vs reduced temperature (see text) showing the kink at the commensurate-incommensurate phase transition, with guides to the eye plotted for each of the two phases. (b) Linewidths λ and λ'. (c) Relaxation rate Λ.

with $\phi = 0$ to the Bessel function form described by Eq. (2) as expected from the incommensurate behavior determined by neutron diffraction.[2] While it is possible to obtain convergent fits to Eq. (1) with ϕ as a free parameter the quality of fit is markedly poorer than for Eq. (2) and the difference is obvious even to the eye. The oscillation frequency f', linewidth λ', and relaxation rate Λ are shown in Figs. 2(a), 2(b), and 2(c), respectively. The linewidth grows more rapidly in this temperature region which suggests that it is dominated by critical fluctuations approaching T_N.

Fitting the oscillation frequencies shown in Fig. 2(a) using Eq. (3), extended to two phases with different β values in each phase but a continuous order parameter, leads to the parameters $T_N = 21.76(1)$ K, $f(0) = 26.57(1)$ MHz, $\alpha = 4.22(5)$, $\beta_C = 0.220(3)$, and $\beta_{IC} = 0.40(5)$, the last two parameters being in the commensurate (C) and incommensurate (IC) ordered phases, respectively. The relaxation rate Λ does not display any clear trend in the ordered phase. Above T_N the data take the exponential form typical of paramagnets where the electronic spin fluctuations are fast compared to the distribution of local fields. The relaxation rate also appears to vary critically above T_N.

In the inset to Fig. 2(a) we show the reduced oscillation frequencies plotted against reduced temperature, taking $f(T = 0)$ and T_N as the fixed points for $F = f(T)/f(0)$ and $t = (T_N - T)/T_N$, respectively. Trends following the expected β values for the two phases are sketched as guides to the eye, without the α parameter used in fitting the trend shown in the main panel. A kink in the plot of F against t is evident at the commensurate-incommensurate phase transition.

B. LiCoPO$_4$

LiCoPO$_4$ has been found to be a model example of a magnet intermediate between 2D and 3D exchange coupling.[41] This gives rise to some unusual critical behavior, with a neutron diffraction study reporting that the temperature dependence of the staggered magnetization follows the form expected for the 2D Ising model and that the critical scattering above $T_N = 22$ K follows a 3D Ising form.[41] The spin waves have also been studied in detail,[42] showing that as well as the dispersions predicted by linear spin wave theory, there is an anomalous dispersionless excitation at $\sim$1.2 meV that was suggested to be related to the magnetoelectric effect in this material.

The form of the raw data for LiCoPO$_4$, shown in Fig. 1(b), is similar to that in the commensurate phase of LiNiPO$_4$ and can be fitted successfully using Eq. (1). However, it was not possible to constrain $\phi = 0$ all the way up to T_N. In such a situation, caution is required in distinguishing between a systematic shift in the time offset of the raw data (arising from an error in determining when muons enter the sample) and a phase offset due to the magnetic field distribution in the sample. Both possibilities were considered in the data analysis. Because the muons were implanted into the sample with their initial spin direction rotated relative to the symmetry axes of the detector system it was possible to use the geometric phase offsets to show that only the phase of the signal was varying with temperature. The data were subsequently analyzed with ϕ as a free parameter, leading to the parameters shown in Fig. 3.

The oscillation frequency shows a smooth, monotonic decrease with increasing temperature and can be fitted to the empirical form of Eq. (3) with the parameters $f(0) = 41.20(1)$ MHz, $T_N = 21.72(1)$ K, $\alpha = 4.91(4)$, and $\beta = 0.299(3)$. This value of β is smaller than that expected for the 3D Ising model ($\beta = 0.326$), but considerably larger than that for the 2D Ising model ($\beta = 0.125$). Vaknin *et al.*[41] compared the results of their neutron diffraction measurements to the analytic Onsager/Yang form[43] $M^{\dagger}(T) = M^{\dagger}(0)[1 - \sinh^{-4}(2J_{2D}/T)]^{1/8}$ for the temperature dependence of the sublattice magnetization in the 2D Ising model, including an additional multiplicative term $\exp[\Delta_{G-E}/(T - T_N)]$, where Δ_{G-E} is the difference between two energies in a two-state model, to describe the interlayer fluctuations relevant near the crossover to 3D behavior. Neither the purely 2D model nor the extended version were able to describe $f(T)$ above 15 K, although the additional multiplicative term does bring the predicted order parameter closer to the trend we observe. We plot the coupled layer model of Ref. 41 as a dashed line in Fig. 3(a) to illustrate this difference. Given the effectiveness of the analytic model below 15 K and the unusually large value of α (dominated by these low-temperature data points), it seems

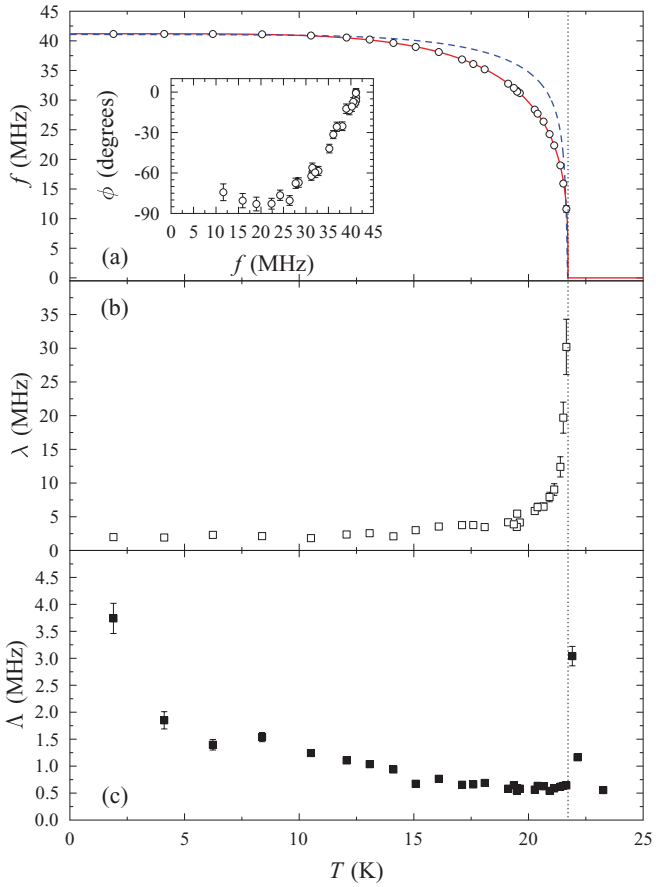

FIG. 3. (Color online) Parameters derived from fitting Eq. (1) to the μSR data for $LiCoPO_4$ shown in Fig. 1(c). (a) Oscillation frequency f with the solid line showing a fit to Eq. (3) and the dashed line showing the model derived in Ref. 41. Inset: Phase of oscillating component ϕ plotted against the oscillation frequency f. This shows that they do not have a monotonic relation, excluding the possibility that a time offset is causing the phase offset. (b) Linewidth λ. (c) Relaxation rate Λ.

that there is a gradual crossover in the effective dimensionality of the system around 15 K that is reflected in the form of the muon data. This is consistent with the 3D fluctuations affecting the muon data at a lower temperature than they affect neutron diffraction data because of the longer timescale probed.

The linewidth λ shown in Fig. 3(b) is slightly larger than in $LiNiPO_4$ at low temperature and appears to grow in two stages as T_N is approached: Around 15 K there is a small step and above 20 K there is a sharper rise associated with critical fluctuations. The relaxation rate Λ shows almost the opposite temperature dependence to λ and is considerably larger than in either of the other two samples. There is no sign of a critical divergence approaching T_N from below and these observations suggest that Λ is dominated by a quasistatic distribution of magnetic fields. Above T_N, Λ shows a more conventional critical divergence.

The temperature dependence of the phase ϕ is plotted in the inset of Fig. 3(a). Below 15 K there is only a slow change in ϕ but it rapidly changes from -10° to $\sim -80^\circ$ above 15 K. This suggests that, approaching T_N, a magnetic inequivalency develops between muon stopping sites in a manner akin to the intermediate phase in $LiNiPO_4$, albeit less pronounced. While a weakly incommensurate structure could generate such an effect, the sharp increase in ϕ occurring at the same temperature as both the departure from the quasi-2D trend in $f(T)$ and the growth in the linewidth suggests that in $LiCoPO_4$ the phase shift comes from increasing disorder in the stacking of the magnetic layers while approaching T_N from below.

C. $LiFePO_4$

$LiFePO_4$ shows a commensurate collinear antiferromagnetic structure below $T_N = 50$ K, with neutron diffraction measurements finding $\beta = 0.27(3)$.[44,45] The Fe moments are orientated slightly away from the b axis, expected on the basis of the crystal symmetry. No evidence for short-range order has been observed above T_N, in contrast to the other members of this series.

The parameters derived from fits of Eq. (1) to the $LiFePO_4$ data are shown in Fig. 4. The temperature dependence of the frequency and linewidth behave conventionally, with $f(T)$ being well described by Eq. (3) with parameters $f(0) = 45.31(2)$ MHz, $T_N = 50.87(7)$ K, $\alpha = 3.66(3)$, and $\beta = 0.381(5)$. This value of β is close to that expected for 3D Heisenberg critical behavior [$\beta = 0.3639(35)$],[46] as opposed to the value of $\beta = 0.27(3)$ previously estimated from neutron scattering measurements.[44,45] The linewidth for $T \ll T_N$ is

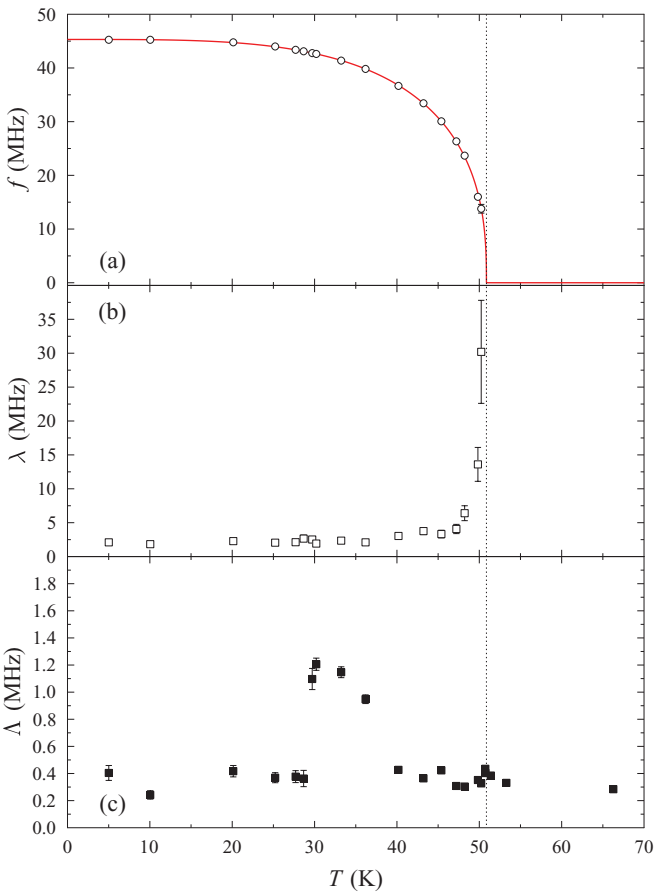

FIG. 4. (Color online) Parameters derived from fitting Eq. (1) to the μSR data for $LiFePO_4$ shown in Fig. 1(b). (a) Oscillation frequency f. (b) Linewidth λ. (c) Relaxation rate Λ.

considerably smaller than the oscillation frequency and it diverges smoothly approaching T_N.

The relaxation rate Λ behaves differently in LiFePO$_4$, compared with the other two samples. There is only a small increase around T_N but the primary feature occurs at 30 K, well below T_N. Associated with this feature is an increase in the relaxing amplitude of the signal as the temperature is increased. Examining the low-temperature data more carefully allows us to identify a further oscillating component with an amplitude around 10% of the primary oscillating component, with an oscillation frequency of ~120 MHz. This component disappears above 30 K and appears to be replaced by the strongly relaxing term that causes an increase in Λ. We can suggest two possible origins for such behavior: Either there is a ~10% FePO$_4$ impurity phase with $T_N \simeq 25$ K,[47] although delithiation is known to lead to a FePO$_4$ phase with $T_N \simeq 125$ K,[44] or this signal corresponds to a muon site which is metastable up to ~30 K. We do not find evidence for a distinct impurity phase and the available data are consistent with a second, metastable muon site.

IV. HIGH-TEMPERATURE RESULTS FOR Li$_x$FEPO$_4$

To investigate the lithium diffusion behavior in Li$_x$FePO$_4$ we measured three samples with $x = 0.8$, 0.9, and 1.0 at temperatures between 75 and 400 K and at fields of 0 and 0.5 mT. By measuring at more than one magnetic field at each temperature it is possible to get a more reliable determination of the fitted parameters, since we have more information on how the field distribution experienced by the muon is decoupled by the field applied parallel to the initial muon spin polarization. Examples of the raw data at the two magnetic fields used are shown in Fig. 5 with the fits described below.

For our high-temperature measurements on Li$_x$FePO$_4$ we assume a Gaussian distribution of random local fields due to the various magnetic moments present in the sample. For a static magnetic system this would lead to a muon depolarization described by the Gaussian Kubo-Toyabe function.[48] Any fluctuations present within the muon time window, which may be caused by either lithium or muon diffusion, can be treated using the strong collision approximation, leading to a dynamic Kubo-Toyabe function.[48] Analysis of the data measured at a series of fields and temperatures using such a dynamic Kubo-Toyabe function proved to be unsuccessful. In studies of lithium-containing battery materials it has been usual to

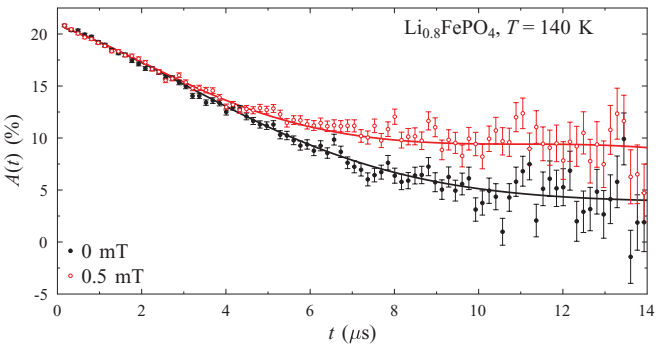

FIG. 5. (Color online) Raw μSR data for Li$_{0.8}$FePO$_4$ at 140 K with fits to Eq. (4) as described in the text.

multiply the dynamic Gaussian Kubo-Toyabe function by an exponential relaxation to eliminate any magnetic contribution to the relaxation.[28,29,32,34] This does not lead to reliable fits to our raw data either. A consistently better quality of fit was obtained by applying Keren's analytic generalization of the Abragam function appropriate for μSR,[49] multiplied by a temperature-independent relaxation rate fixed for each sample:

$$P_z(t) = \exp[-\Gamma(\Delta,\nu,\omega_L,t)t]\exp(-\lambda t), \qquad (4)$$

where $\Gamma(\Delta,\nu,\omega_L,t)$ is defined in Eq. (4) of Ref. 49. This describes the muon polarization having subtracted a fixed background signal. The parameter Δ describes the quasistatic distribution of field at the muon stopping site, ν is the temperature-dependent fluctuation rate, $\omega_L = \gamma_\mu B$ is the muon's Larmor precession frequency in the applied magnetic field, and λ is due to temperature-independent fluctuations. (After initial unconstrained fits had been made, λ values were fixed at 0.05, 0.02, and 0.1 MHz for the $x = 0.8$, 0.9, and 1.0 samples, respectively.) In the $x = 0.9$ sample we found a strong temperature-independent relaxation coming from a minority phase which could be subtracted from the data analysis using $A_m \exp(-\Lambda t)$, with the values of Λ shown in the inset to Fig. 6(b). The values of Δ and ν obtained from these fits are shown in Figs. 6(a) and 6(b), respectively.

The Δ values in Fig. 6(a) show the trend observed in the vast majority of lithium-containing battery materials investigated to date for $x = 0.9$, where a low-temperature plateau is followed by a smooth decrease to a high-temperature plateau.[28,29,32,34] In the $x = 0.8$ and 1 samples there is a peak at around the temperature where the low-temperature plateau ends in the $x = 0.9$ sample. The values of $\Delta \sim 0.2$ MHz are broadly similar to those in Li$_x$CoO$_2$,[28] LiMn$_2$O$_4$,[29] and Li$_{1-x}$Ni$_{1+x}$O$_2$,[34] but smaller than in Li$_{3-x-y}$Ni$_x$N.[32]

The temperature dependence of ν follows a similar trend in each sample, with a slight fall from the lowest measured temperature to around 100 K, followed by a smooth rise toward ~250 K, and then a sharp drop-off to either the low-temperature value, or in $x = 0.8$, to the value at the peak. It seems likely that the change observed below 100 K is due to the buildup of magnetic correlations that are not well described by our temperature-independent λ value. Above 100 K the thermally activated growth in the hopping rate mirrors that observed in Li$_x$CoO$_2$[28] and Li$_{1-x}$Ni$_{1+x}$O$_2$,[34] albeit with a different temperature scale. The behavior above the peak at ~250 K may be related to the onset of muon hopping, but this may not be a unique explanation.

Comparing our results to those obtained previously naturally leads to the question of whether the phenomena we observe are associated with the diffusion of lithium and/or muons. The similarity of the temperature dependencies of both Δ and ν to previous results on other materials indeed suggest that they are caused by the same phenomenon. This leaves the further question of whether we can obtain quantitative information about the lithium diffusion from our results. While we could not use the dynamic Gaussian Kubo-Toyabe function multiplied by an exponential used in Refs. 28, 29, and 34, the modified Keren function we have employed provides the same information and a more robust fit of our data over the whole measured temperature range. That ν follows an

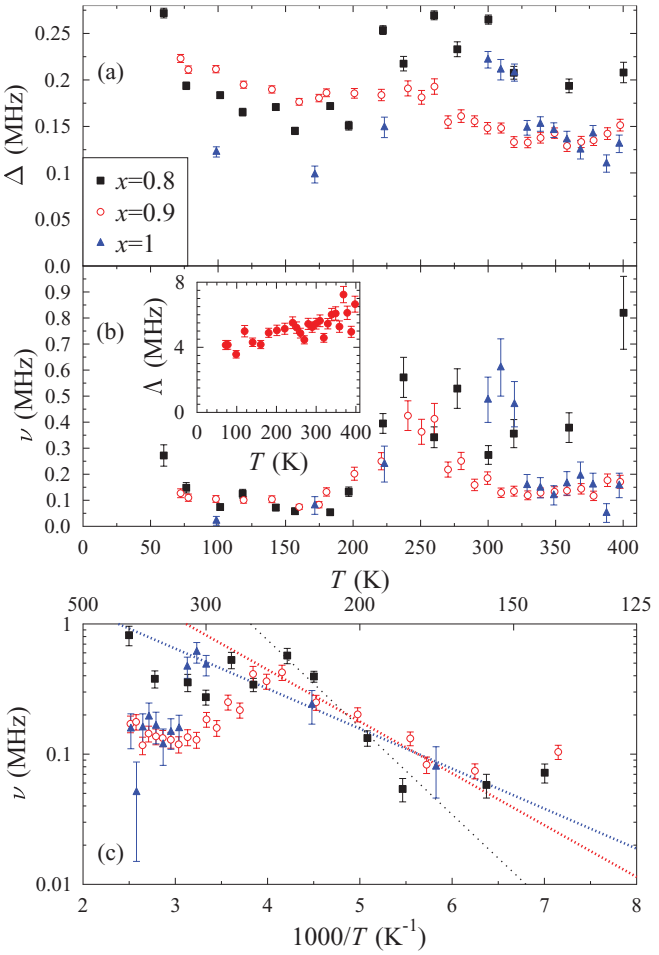

FIG. 6. (Color online) Parameters derived from fitting Eq. (4) to the μSR data for Li_xFePO_4. (a) Field distribution width Δ. (b) Fluctuation rate ν. Inset: Relaxation rate Λ for $Li_{0.9}FePO_4$. (c) Fluctuation rate ν plotted against the inverse temperature to illustrate the thermally activated behavior below about 250 K. The lines plotted are fits to the data in the activated region with parameters described in the text.

activated temperature dependence over a similar temperature range to that observed in other materials, as is illustrated in Fig. 6(c), strongly suggests that up to around 250 K we can assign the change in ν to lithium diffusion. Above this temperature it is likely that the muons become mobile and this results in either a drop in Δ or ν as the form of the data changes.

Arrhenius fits to ν over the thermally activated region allow us to estimate the energy barriers E_a for lithium diffusion, which for $x = 0.8$, 0.9, and 1.0 are 130(10), 80(10), and 60(10) meV, respectively. Extrapolating the fits to 300 K for comparison with other measured values gives us estimates of the lithium hopping rate at room temperature of 2×10^6 s^{-1} ($x = 0.8$), 0.8×10^6 s^{-1} ($x = 0.9$), and 0.5×10^6 s^{-1} ($x = 1.0$). (The extrapolation to room temperature introduces an error of ~50% in these values whereas the individual points within the measured range have errors around 10%.)

Taking the primary hopping pathway to be along the b axis[20,50] we can further estimate the diffusion constant for $LiFePO_4$. The distance traveled in each hop will be $b/2$ and this leads to a diffusion constant $D_{Li} = b^2\nu/4$. Given these assumptions we estimate $D_{Li} = 1.9 \times 10^{-9}$ cm^2 s^{-1} for the $x = 0.8$ sample, and 7.6×10^{-10} cm^2 s^{-1} and 4.6×10^{-10} cm^2 s^{-1} for the $x = 0.9$ and $x = 1.0$ samples, respectively.

TABLE I. Comparison of reported estimates for D_{Li} and E_a obtained using different techniques (at room temperature unless noted). A more detailed list of E_a values is given in Ref. 18.

Technique	D_{Li} (cm^{2}s^{-1})	E_a (meV)
μSR (this study)	10^{-10} to 10^{-9}	~100
Mössbauer spectroscopy[10]	10^{-7}	775 ± 108[a]
Mössbauer spectroscopy[11]	10^{-13} to 10^{-11}	335 ± 25[b]
Titration and ac impedance[12]	10^{-15}	
Titration[13]	10^{-16} to 10^{-10}	
Impedance[14]	10^{-14}	
Cyclic voltammetry[15]	10^{-14}	400
First-principles calculations[16]	10^{-8}	270
First-principles calculation[17]		550
AC and DC conductivity[18]		620–740
AC impedance[19]		155
AC impedance (a axis)[20]		636(52)
AC impedance (b axis)[20]		540(48)
AC impedance (c axis)[20]		669(54)
Electrochemistry[21]		155

[a]Determined around 600 K.
[b]Determined around 450 K.

We can compare our estimates for the activation barrier and diffusion constant to those derived from other techniques, which are summarized in Table I. Most theoretical work and experiments find E_a for lithium diffusion within the range 600–750 meV,[10,18,20,23,51,52] although there is both theoretical and experimental evidence for E_a ~ 100–300 meV.[16,19,21,53] Smaller energy barriers have been suggested for the electronic conduction via the hopping of small polarons and it has been argued that the polaron hopping may be correlated with the hopping of lithium ions.[10,22,23] The activation energy of ~100 meV that we observe suggests that the hopping process observed by the muons is unlikely to be associated with a barrier as large as 600 meV and this suggests that another, perhaps correlated, process facilitates lithium diffusion at lower temperatures. It is conceivable that bulk measurements are more sensitive to mesoscopic barriers beyond the length scale investigated by muons.

The disparity between measurements of D_{Li} from different techniques is far greater than that seen for E_a, with values ranging from 10^{-16} to 10^{-7} cm^2 s^{-1}.[10,12–15] Theoretical work[16] and local measurements, such as Mössbauer spectroscopy,[10,11] seem to give larger values of D_{Li} ~ 10^{-13} to 10^{-7} cm^2 s^{-1} than bulk measurements, which give D_{Li} ~ 10^{-16} to 10^{-10} cm^2 s^{-1} (Ref. 13). Our estimate lies within the overlap of these groups. This suggests that there is a difference between microscopic and bulk determinations of D_{Li} which could result from the effect of the $LiFePO_4/FePO_4$ phase boundary motion or mesoscopic barriers to lithium diffusion such as the blocking of diffusion channels by Fe_{Li} defects and grain boundaries, the latter accentuated by the habit of crystallites to be platelets with the b axis as their shortest dimension.

V. CONCLUSION

We have used μSR to provide a new window on both the magnetic and diffusive properties of this series of olivine phosphates. This has shown how the commensurate-incommensurate phase transition in $LiNiPO_4$ occurs without a discontinuity in the internal field at the muon stopping site; how the nature of the fluctuations approaching T_N in $LiCoPO_4$ are more three-dimensional in the muon time window than those found to be quasi-two dimensional in neutron scattering measurements; and that the ordering of $LiFePO_4$ is more conventional than that of the other two materials studied, though again the three-dimensional fluctuations are more evident in determining the behavior of the order parameter approaching T_N. Our measurements also provide a new means of investigating the process of lithium diffusion in Li_xFePO_4, finding a diffusion constant $D_{Li} \sim 10^{-10}$ to 10^{-9} cm^2 s^{-1} and an energy barrier of $E_a \sim 100$ meV.

Shortly before we submitted this paper Ref. 54 was published reporting analogous measurements of $LiFePO_4$. Two oscillating components and a fast-relaxing component were observed to extend up to T_N suggesting that the higher frequency component may originate in a metastable muon site or nearly degenerate muon sites between which the muon hops. The high-temperature data were parameterized slightly differently but led to nearly identical values of both D_{Li} and E_a.

ACKNOWLEDGMENTS

Parts of this work were performed at the Swiss Muon Source, Paul Scherrer Institute, Villigen, Switzerland, and the ISIS Facility, UK. We thank A. Amato for experimental assistance, S. Hull for helpful discussions, and the EPSRC and STFC (UK) for financial support.

*peter.baker@stfc.ac.uk

[1] S. Geller and J. L. Durand, Acta Crystallogr. **13**, 325 (1960).
[2] D. Vaknin, J. L. Zarestky, J.-P. Rivera, and H. Schmid, Phys. Rev. Lett. **92**, 207201 (2004).
[3] I. Kornev, M. Bichurin, J.-P. Rivera, S. Gentil, H. Schmid, A. G. M. Jansen, and P. Wyder, Phys. Rev. B **62**, 12247 (2000).
[4] B. B. Van Aken, J.-P. Rivera, H. Schmid, and M. Fiebig, Nature (London) **449**, 702 (2007).
[5] A. K. Padhi, K. S. Nanjundaswamy, and J. B. Goodenough, J. Electrochem. Soc. **144**, 1188 (1997).
[6] A. Yamada, S. C. Chung, and K. Hinokuma, J. Electrochem. Soc. **148**, A224 (2001).
[7] M. S. Whittingham, Y. Song, S. Lutta, P. Y. Zavalij, and N. A. Chernova, J. Mater. Chem. **15**, 3362 (2005).
[8] T. Ohzuku and R. Brodd, J. Power Sources **174**, 449 (2007).
[9] L.-X. Yuan, Z.-H. Wang, W.X. Zhang, X.-L. Hu, J.-T. Chen, Y.-H. Huang, and J. B. Goodenough, Energy Environ. Sci. **4**, 269 (2011).
[10] B. Ellis, L. K. Perry, D. H. Ryan, and L. F. Nazar, J. Am. Chem. Soc. **128**, 11416 (2006).
[11] J. L. Dodd, I. Halevy, and B. Fultz, J. Phys. Chem. C **111**, 1563 (2007).
[12] P. P. Prosini, M. Lisi, D. Zane, and M. Pasquali, Solid State Ionics **148**, 45 (2002).
[13] A. V. Churikov, A. V. Ivanishchev, I. A. Ivanishcheva, V. O. Sycheva, N. R. Khasanova, and E. V. Antipov, Electrochem. Acta **55**, 2939 (2010).
[14] S. Franger, F. Le Cras, C. Bourbon, and H. Rouault, Electrochem. Solid-State Lett. **5**, A231 (2002).
[15] D. Y. W. Yu, C. Fietzek, W. Weydanz, K. Donoue, T. Inoue, H. Kurokawa, and S. Fujitani, J. Electrochem. Soc. **154**, A253 (2007).
[16] D. Morgan, A. Van der Ven, and G. Ceder, Electrochem. Solid State Lett. **7**, A30 (2004).
[17] M. S. Islam, D. J. Driscoll, C. A. J. Fisher, and P. R. Slater, Chem. Mater. **17**, 5085 (2005).
[18] R. Amin, J. Maier, P. Balaya, D. P. Chen, and C. T. Lin, Solid State Ionics **179**, 1683 (2008).
[19] M. Takahashi, S. Tobishima, K. Takei, and Y. Sakurai, Solid State Ionics **148**, 283 (2002).
[20] J. Li, W. Yao, S. Martin, and D. Vaknin, Solid State Ionics **179**, 2016 (2008).
[21] C. Wang and J. Hong, Electrochem. Solid-State Lett. **10**, A65 (2007).
[22] T. Maxisch, F. Zhou, and G. Ceder, Phys. Rev. B **73**, 104301 (2006).
[23] K. Hoang and M. Johannes, Chem. Mater. **23**, 3003 (2011).
[24] J. Cabana, J. Shirakawa, G. Chen, T. J. Richardson, and C. P. Grey, Chem. Mater. **22**, 1249 (2010).
[25] S. J. Blundell, Contemp. Phys. **40**, 175 (1999).
[26] A. Yaouanc and P. D. de Réotier, *Muon Spin Rotation, Relaxation, and Resonance* (Oxford University Press, Oxford, 2011).
[27] R. Kadono, J. Imazato, T. Matsuzaki, K. Nishiyama, K. Nagamine, T. Yamazaki, D. Richter, and J.-M. Welter, Phys. Rev. B **39**, 23 (1989).
[28] J. Sugiyama, K. Mukai, Y. Ikedo, H. Nozaki, M. Månsson, and I. Watanabe, Phys. Rev. Lett. **103**, 147601 (2009).
[29] C. T. Kaiser, V. W. J. Verhoeven, P. C. M. Gubbens, F. M. Mulder, I. de Schepper, A. Yaouanc, P. Dalmas de Réotier, S. P. Cottrell, E. M. Kelder, and J. Schoonman, Phys. Rev. B **62**, R9236 (2000).
[30] M. J. Ariza, D. J. Jones, J. Rozière, J. S. Lord, and D. Ravot, J. Phys. Chem. B **107**, 6003 (2003).
[31] P. C. M. Gubbens, M. Wagemaker, S. Sakarya, M. Blaauw, A. Yaouanc, P. Dalmas de Réotier, and S. P. Cottrell, Solid State Ionics **177**, 145 (2006).
[32] A. S. Powell, J. S. Lord, D. H. Gregory, and J. J. Titman, J. Phys. Chem. C **113**, 20758 (2009).
[33] K. Mukai, J. Sugiyama, Y. Ikedo, H. Nozaki, K. Shimomura, K. Nishiyama, K. Ariyoshi, and T. Ohzuku, J. Power Sources **174**, 711 (2007).
[34] J. Sugiyama, Y. Ikedo, K. Mukai, H. Nozaki, M. Månsson, O. Ofer, M. Harada, K. Kamazawa, Y. Miyake, J. H. Brewer, E. J. Ansaldo, K. H. Chow, I. Watanabe, and T. Ohzuku, Phys. Rev. B **82**, 224412 (2010).
[35] V. W. J. Verhoeven, I. M. de Schepper, G. Nachtegaal, A. P. M. Kentgens, E. M. Kelder, J. Schoonman, and F. M. Mulder, Phys. Rev. Lett. **86**, 4314 (2001).
[36] K. Nakamura, H. Ohno, K. Okamura, Y. Michihiro, T. Moriga, I. Nakabayashi, and T. Kanashiro, Solid State Ionics **177**, 821 (2006).
[37] F. L. Pratt, Physica B **289-290**, 710 (2000).

[38] Yu. N. Kharchenko, N. F. Kharcheno, M. Baran, and R. Szymczak, Low Temp. Phys. **29**, 579 (2003).
[39] D. Vaknin, J. L. Zarestky, J. E. Ostenson, B. C. Chakoumakos, A. Goñi, P. J. Pagliuso, T. Rojo, and G. E. Barberis, Phys. Rev. B **60**, 1100 (1999).
[40] T. B. S. Jensen, N. B. Christensen, M. Kenzelmann, H. M. Rønnow, C. Niedermayer, N. H. Andersen, K. Lefmann, M. Jiménez-Ruiz, F. Demmel, J. Li, J. L. Zarestky, and D. Vaknin, Phys. Rev. B **79**, 092413 (2009).
[41] D. Vaknin, J. L. Zarestky, L. L. Miller, J.-P. Rivera, and H. Schmid, Phys. Rev. B **65**, 224414 (2002).
[42] W. Tian, J. Li, J. W. Lynn, J. L. Zarestky, and D. Vaknin, Phys. Rev. B **78**, 184429 (2008).
[43] L. Onsager, Phys. Rev. **65**, 117 (1944); C. N. Yang, *ibid*. **85**, 809 (1952).
[44] G. Rousse, J. Rodriguez-Carvajal, S. Patoux, and C. Masquelier, Chem. Mater. **15**, 4082 (2003).
[45] J. Li, V. O. Garlea, J. L. Zarestky, and D. Vaknin, Phys. Rev. B **73**, 024410 (2006).
[46] K. Chen, A. M. Ferrenberg, and D. P. Landau, Phys. Rev. B **48**, 3249 (1993).
[47] P. D. Battle, A. K. Cheetham, C. Gleitzer, W. T. A. Harrison, G. J. Long, and G. Longworth, J. Phys. C **15**, L919 (1982).
[48] R. S. Hayano, Y. J. Uemura, J. Imazato, N. Nishida, T. Yamazaki, and R. Kubo, Phys. Rev. B **20**, 850 (1979).
[49] A. Keren, Phys. Rev. B **50**, 10039 (1994).
[50] S. Nishimura, G. Kobayashi, K. Ohoyama, R. Kanno, M. Yashima, and A. Yamada, Nature Mater. **7**, 707 (2008).
[51] C. Delacourt, P. Poizot, J.-M. Tarascon, and C. Masquelier, Nature Mater. **4**, 254 (2005).
[52] J. Molenda, W. Ojczyk, K. Swierczek, W. Zajac, F. Krok, J. Dygas, and R.-S. Liu, Solid State Ionics **177**, 2617 (2006).
[53] S. Q. Shi, L. J. Liu, C. Y. Ouyang, D. S. Wang, Z. X. Wang, L. Q. Chen, and X. J. Huang, Phys. Rev. B **68**, 195108 (2003).
[54] J. Sugiyama, H. Nozaki, M. Harada, K. Kamazawa, O. Ofer, M. Månsson, J. H. Brewer, E. J. Ansaldo, K. H. Chow, Y. Ikedo, Y. Miyake, K. Ohishi, I. Watanabe, G. Kobayashi, and R. Kanno, Phys. Rev. B **84**, 054430 (2011).